

The ultrafast onset of exciton formation in 2D semiconductors

Chiara Trovatello¹, Florian Katsch², Nicholas J. Borys^{3,4,5}, Malte Selig², Kaiyuan Yao^{3,4,6}, Rocio Borrego-Varillas⁷, Francesco Scotognella¹, Ilka Kriegel⁸, Aiming Yan^{9,10,11,#}, Alex Zettl^{9,10,11}, P. James Schuck^{3,4,6}, Andreas Knorr², Giulio Cerullo^{1,7} and Stefano Dal Conte¹

¹*Dipartimento di Fisica, Politecnico di Milano, Piazza L. da Vinci 32, I-20133 Milano, Italy*

²*Institut für Theoretische Physik, Technische Universität Berlin, Berlin, 10623, Germany*

³*Molecular Foundry Division, Lawrence Berkeley National Laboratory, Berkeley, California 94720, USA*

⁴*Department of Mechanical Engineering, University of California, Berkeley, California 94720, USA*

⁵*Department of Physics, Montana State University, Bozeman, MT USA*

⁶*Department of Mechanical Engineering, Columbia University, New York, New York 10027, USA*

⁷*IFN-CNR, Piazza L. da Vinci 32, I-20133 Milano, Italy*

⁸*Department of Nanochemistry, Istituto Italiano di Tecnologia (IIT), via Morego, 30, 16163 Genova, Italy*

⁹*Department of Physics, University of California at Berkeley, Berkeley, California 94720, USA*

¹⁰*Materials Sciences Division, Lawrence Berkeley National Laboratory, Berkeley, California, 94720, USA*

¹¹*Kavli Energy NanoSciences Institute at the University of California, Berkeley and the Lawrence Berkeley National Laboratory, Berkeley, California 94720, USA*

Present address: Department of Physics, University of California at Santa Cruz, Santa Cruz, California, 95064 U.S.A.

** Corresponding Author: Stefano Dal Conte, Giulio Cerullo, Andreas Knorr*

*Email address: stefano.dalconte@polimi.it, giulio.cerullo@polimi.it,
andreas.knorr@tu-berlin.de*

The equilibrium and non-equilibrium optical properties of single-layer transition metal dichalcogenides (TMDs) are determined by strongly bound excitons. Exciton relaxation dynamics in TMDs have been extensively studied by time-domain optical spectroscopies. However, the formation dynamics of excitons following non-resonant photoexcitation of free electron-hole pairs have been challenging to directly probe because of their inherently fast timescales. Here we use extremely short optical pulses to non-resonantly excite an electron-hole plasma and show the formation of two-dimensional excitons in single-layer MoS₂ on the timescale of 30 fs via the induced changes to photo-absorption. These formation dynamics are significantly faster than in conventional 2D quantum wells and are attributed to the intense Coulombic interactions present in 2D TMDs. A theoretical model of a coherent polarization that dephases and relaxes to an incoherent exciton population reproduces the experimental dynamics on the sub-100-fs timescale and sheds light into the underlying mechanism of how the lowest-energy excitons, which are the most important for optoelectronic applications, form from higher-energy excitations. Importantly, a phonon-mediated exciton cascade from higher energy states to the ground excitonic state is found to be the rate-limiting process. These results set an ultimate timescale of the exciton formation in TMDs and elucidate the exceptionally fast physical mechanism behind this process.

I. INTRODUCTION

Single-layer (1L) TMDs are attracting growing interest because of their peculiar properties that make them highly suitable for optoelectronics applications [1]. The reduced dielectric screening that is caused by the strong spatial confinement, results in an optical response that is dominated even at room temperature by strongly bound excitons with large (hundreds of meV) binding energies [2, 3]. The enhanced Coulomb interaction gives rise to additional effects such as the occurrence of a Rydberg series of excitonic states [4] and many body complexes like trions [5] and biexcitons [6], whose physical properties can be tuned by changing the dielectric environment [7] or by applying external stimuli such as light [8], strain [9], electric [10] and magnetic fields [11]. Ultrashort laser pulses offer an ad-

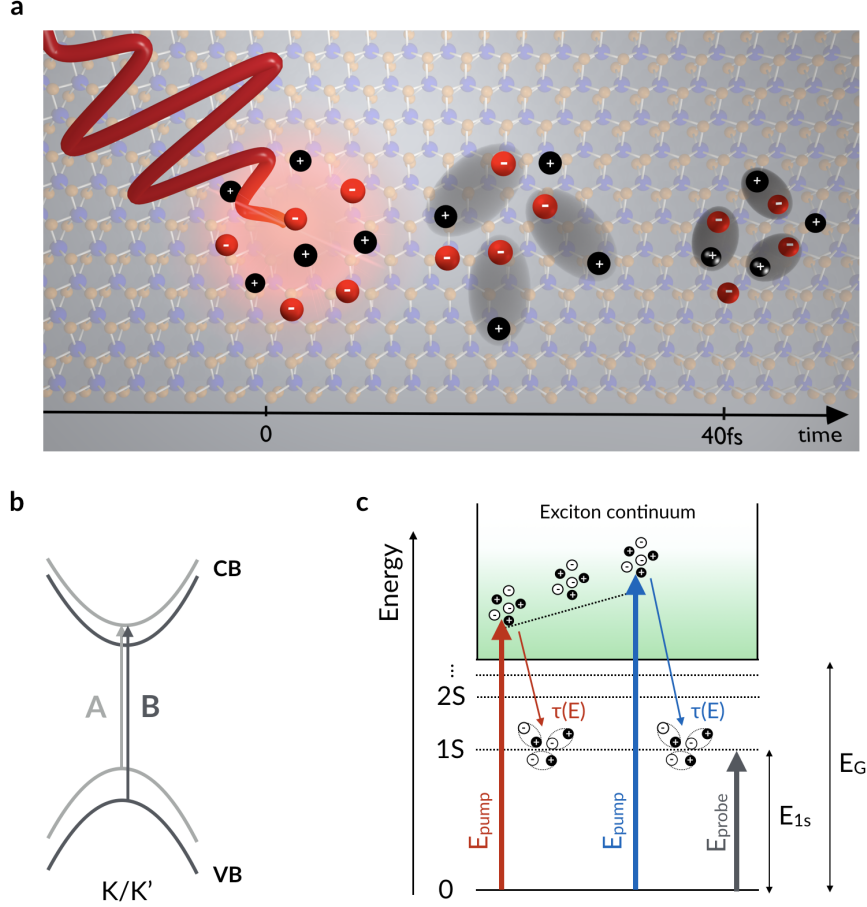


FIG. 1: **Exciton formation process in 1L-MoS₂.** a) Cartoon of the exciton formation process after photo-injection of free electron-hole pairs. b) Schematic illustration of the single particle band structure of 1L-MoS₂ at the K/K points. The two arrows represent A/B excitonic transitions, split due to the strong spin-orbit interaction at the K/K' points of the Brillouin zone. c) Sketch of the pump-probe experiment. A few-optical-cycle laser pulse injects free electron/hole pairs at increasing energies above the exciton continuum (E_G). These quasiparticles lose their initial kinetic energy and scatter down, via a cascade process, to lower-lying discrete excitonic states until they reach the 1S excitonic state. The timescale $\tau(E)$ of this relaxation process is determined by measuring the absorption change of a probe beam, tuned on resonance with the 1S state, due to the Pauli blocking effect.

ditional way to change and potentially control the properties of excitons on a fast timescale. The non-equilibrium optical response of TMDs has been extensively explored both experimentally and theoretically [12, 13]. The dynamical response of TMDs and in general all semiconductors can be divided into coherent and incoherent regimes [14, 15]. While the

incoherent exciton dynamics of TMDs, including processes such as exciton thermalization [16], radiative/non radiative recombination [17], intra and intervalley scattering [18–22], exciton dissociation [23] and exciton-exciton annihilation [24] have been extensively studied, the coherent exciton response and the corresponding early stage dynamics of the exciton formation process are still almost unexplored largely because the limited available temporal resolution (i.e. > 100 fs for pump-probe optical spectroscopy and > 1 ps for time-resolved photoluminescence) has prevented the study of the primary early stage dynamics of exciton photo-generation processes [17, 26].

Here, we push the temporal resolution of ultrafast differential reflectivity ($\Delta R/R$) spectroscopy to the regime of less than 30 fs in order to investigate the dynamics of exciton formation in 1L-MoS₂. Experimentally, we employ a pump-probe technique that uses $\Delta R/R$ to monitor the evolution of the excited state population. Particularly, we elucidate how long it takes for an initial population of high-energy photoexcited electrons and holes to relax to the lowest-energy exciton states (i.e., the 1S states of the A and B excitons), and how this formation time depends upon the energy of the initial state (c.f. Fig.1). The measured dynamics are found to be remarkably fast, suggesting that lowest-energy excitons form from these high energy populations with a characteristic timescale as fast as 10 fs. Upon increasing the energy of the initial state of photoinjected carriers (i.e., by increasing the pump photon energy), we find that (1) the formation time of the excitons increases linearly with increasing energy; (2) an initial, sub-100 fs fast decay component of the excitons vanishes; and (3) the dynamics of a slower decay process (on the timescale of picoseconds) associated with the relaxation of a thermal population of excitons does not substantially change. Simulations based on the TMD Bloch equations attribute the excitation energy dependence of the formation dynamics to a phonon-induced cascade-like relaxation process of high-energy incoherent excitons down to the excitonic ground state [25]. This process, although extremely fast, is predicted to have a characteristic time constant between 20 and 30 fs, corroborating our experimental observations. The early sub-100 fs relaxation dynamics are also well captured by the simulations, which reveal that they arise from the decay of the pump-induced coherent optical polarization into ultimately thermal exciton populations (i.e., incoherent excitons). These results are of great relevance for optoelectronic applications of TMDs as they directly define a timescale for an efficient extraction of hot carriers in 1L-TMDs and TMD-based heterostructures before the exciton

formation process.

II. RESULTS AND DISCUSSION

Figure 1 schematically summarizes the exciton formation process (Fig.1a) and the key optical excitonic transitions (Figs 1b) of 1L-MoS₂. The 1L-MoS₂ used here is grown by chemical vapor deposition on a SiO₂/Si substrate. All measurements were made on as-grown samples. From the steady-state reflectance measurements that are reported in Supplementary Fig. S1, the lowest energy A and B excitonic resonances that arise from optical transitions between the two-highest energy valence bands and the lowest-energy conduction bands at the K and K' points in the Brillouin zone are centered at the energies of 1.88 eV and 2.03 eV, respectively (see sketch in Fig. 1b). As illustrated in Fig. 1c, both the A and B optical transitions form two manifolds of Rydberg-like series of bound states that merge into a continuum of unbound electron-hole states [3, 27]. These resonances correspond to the lowest-energy (or ground-state) excitons in the A and B manifolds (i.e., the A_{1s} and B_{1s} states, respectively), possess the largest oscillator strengths, and dominate the optical response over the corresponding higher-energy unbound states. Based on previous experimental studies [3, 27] and refined theoretical models [18], we estimate that the exciton binding energy (i.e., the energetic difference between the 1S exciton and the lowest energy state in the exciton continuum) is of the order of 350 meV. In our measurements the pump photon energies span from 2.29 eV to 2.75 eV (with bandwidths spanning from 90 to 120 meV) and thus, at all energies, photoexcitation predominantly creates an initial population of excitons at or well-into the exciton continuum for the A excitons (as well as for the B excitons at energies above ~ 2.4 eV). To monitor the formation dynamics and quantify the formation time (i.e. $\tau(E)$ in Fig. 1c), our probe energies monitor the rise and decay dynamics of the $\Delta R/R$ signals for the 1S states of the A and B excitons.

We use tunable pump pulses to photo-inject electron-hole pairs with increasing excess energy with respect to E_G . The time-delayed broadband probe pulses measure the build-up and early decay dynamics of both A_{1s} and B_{1s} excitons. The experimental temporal resolution of the setup is sub-30-fs (see Methods and Supplementary Fig.S4). Figures 2a and 2b report $\Delta R/R(E_{probe}, \tau)$ maps as function of the pump-probe delay τ and the probe

photon energy E_{probe} for two different pump photon energies: 2.29 eV and 2.75 eV, i.e. respectively across and well above E_G . Due to the presence of the reflecting Si substrate, $\Delta R/R$ is equivalent to a double-pass differential transmission ($\Delta T/T$). Both measurements show comparable qualitative responses: positive strong features associated with the A_{1s} (centered at $E_{probe} = 1.88$ eV) and B_{1s} (centered at $E_{probe} = 2.03$ eV) exciton states. In the temporal window explored in the experiment (i.e. ~ 200 fs), the $\Delta R/R$ spectrum displays a symmetric profile around each excitonic resonance with no shift of the peak maximum, showing that the signal is dominated by Pauli blocking (see Supplementary Fig.S2).

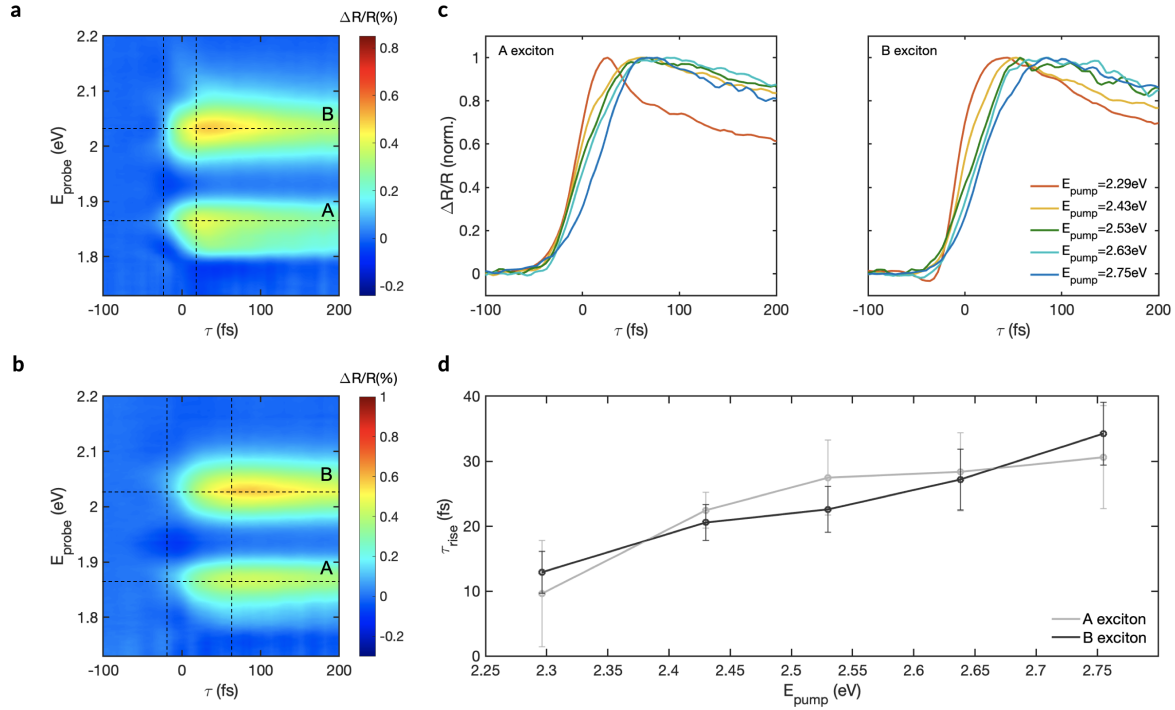


FIG. 2: **Energy dependent exciton formation process.** $\Delta R/R$ maps measured on 1L-MoS₂ photo-excited a) at 2.29eV and b) at 2.75eV. The measurements are performed at room temperature. The horizontal dashed lines pass through the maximum of the $\Delta R/R$ spectrum at the energies of the A_{1s}/B_{1s} exciton transitions, while the vertical lines mark the temporal range from 10% to 90% of the build-up signal. The excitation fluence is $50\mu J/cm^2$. Pump and probe beams are linearly polarized. The time zero is defined, for each measurement, as the maximum of the cross correlation signal between the pump and the probe pulses as explained in the Methods. c-d) Temporal cuts of the $\Delta R/R$ maps measured across the A_{1s} and B_{1s} excitonic resonances for increasing pump photon energy. e) Pump photon energy dependence of τ_{rise} . The error bars are obtained from the fits of the time traces.

A closer inspection of the maps reveals that the formation time τ_{rise} of the $\Delta R/R$ signals of the A_{1s} and B_{1s} excitons is longer for higher pump photon energies. When the excitation energy is close to E_G , the signal displays a quasi-instantaneous (i.e. pulse-width limited) build-up, while for increased pump photon energy τ_{rise} significantly increases. We stress that this result can be observed only thanks to the high temporal resolution of the setup. To better quantify this effect, Fig.2c reports the temporal cuts of the maps taken at the A_{1s} exciton peak for increasing pump photon energies. Figure 2d reports similar cuts for the B_{1s} exciton. The precise timescale of the build-up dynamics is determined by fitting the time traces in Fig.2c with the product of a rising exponential (accounting for the finite τ_{rise}) and a decaying exponential that is convoluted with a Gaussian function which accounts for the finite pulse duration. Details on the fitting procedure are given in Supplementary Note 5. Figure 2e unambiguously shows that τ_{rise} monotonically increases with the initial excess energy of the photoinjected carriers. Another interesting effect is the extremely fast decay observed at lower pump photon energy, which occurs on a time-scale comparable to that of the build-up and fades away as the pump is tuned to higher photon energies. This effect is particularly clear on the A exciton $\Delta R/R$ trace (see Fig.2c).

To identify the essential mechanisms that underlie the early-time non-equilibrium optical response of 1L-MoS₂, we performed simulations based on the TMD Bloch equations[29]. Our model describes the temporal dynamics of the excitons after the photoexcitation of free electron-hole pairs above or close to E_G . The bleaching contribution to the pump-probe signal at the A/B exciton transitions, due to the photoexcitation process, is also calculated and compared with experimental results. Excitonic excitations are theoretically described by solving the Wannier equation (see Supplementary Note 7) [28, 29]. The exciton kinetics are determined by a set of coupled differential equations (TMD Bloch equations) describing the temporal evolution of the polarization (in our theory an excitonic scattering state) and the excitonic population (incoherent excitons) where the phonon-mediated relaxation from energetically higher densities is described with effective rates $\Gamma_{\nu+1 \rightarrow \nu}$ determined by independent density functional theory calculations (see Methods section). Solving the set of equations of motion for the coherent polarization as well as incoherent exciton population gives access to the Pauli-blocking contributions of the measured differential signal at the 1s exciton resonance frequencies.

The results of the simulations, reported in Fig.3a, agree remarkably well with the

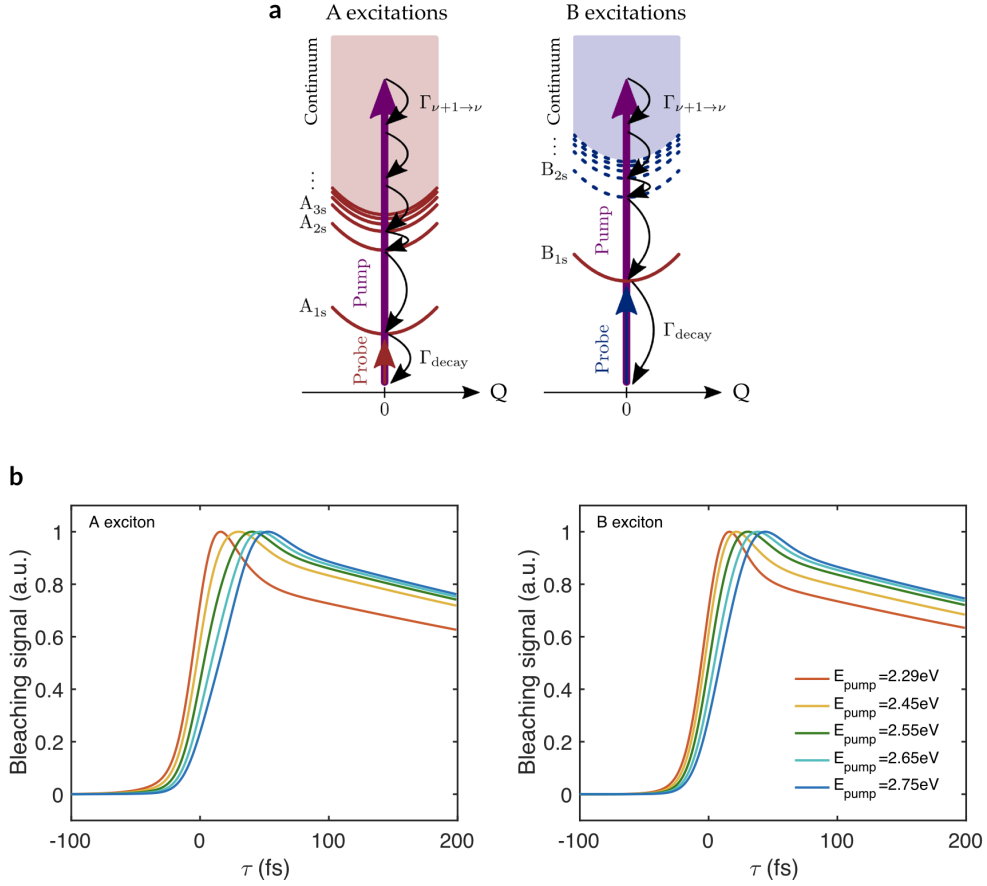


FIG. 3: **Simulation of the exciton formation process.** a) Schematic illustration of the relaxation model in the exciton picture. After optical excitation of continuum states with the pump pulse the sample is probed at the A_{1s} (left) and B_{1s} (right) exciton resonance energy. The measured signal exhibits contributions originating from instantaneous coherent polarizations as well as incoherent exciton densities which are formed in the continuum and relax down to the energetically lowest 1s states (relaxation rate $\Gamma_{\nu+1\rightarrow\nu}$). Finally, the exciton density associated with the lowest 1s states decays slowly with a rate Γ_{decay} . b) Calculated Pauli blocking contributions to the pump-probe signals at the A_{1s} (left) and B_{1s} (right) exciton resonance energy for varying pump photon energies. All the calculated traces are normalized to the maximum value.

experimental results. For all pump photon energies, the calculated bleaching signal exhibits sub-100-fs build-up followed by a decay time on the picosecond timescale. At higher pump energies, the peak of the signal is progressively delayed as a result of a slower rise time. The timescale and the pump photon energy dependence of the build-up dynamics are in remarkable quantitative agreement with the experimental results. The slowing of τ_{rise} with increasing pump photon energy is the result of a high-energy exciton cascade scattering

process down to the excitonic ground state. A sketch of the scattering processes involving photoexcited excitons is reported in Fig.3b. The non-resonant pump pulse induces an almost instantaneous coherent interband exciton polarization which oscillates with the same frequency of the driving pulse. This polarization rapidly dephases by exciton-phonon scattering and leads to a delayed formation of an incoherent exciton population involving electronic states above E_G [14]. These high-energy weakly bound excitons quickly lose their energy and decay into lower lying continuum and discrete excitonic states. The scattering process continues until most of the excitonic population reaches the lowest energy 1S exciton state. With increasing pump photon energy, the number of intermediate scattering events, required to complete the cascade process, increases. This increase in needed scattering events results in the experimentally observed delayed formation of the bleaching signal measured at the A_{1s}/B_{1s} optical transitions.

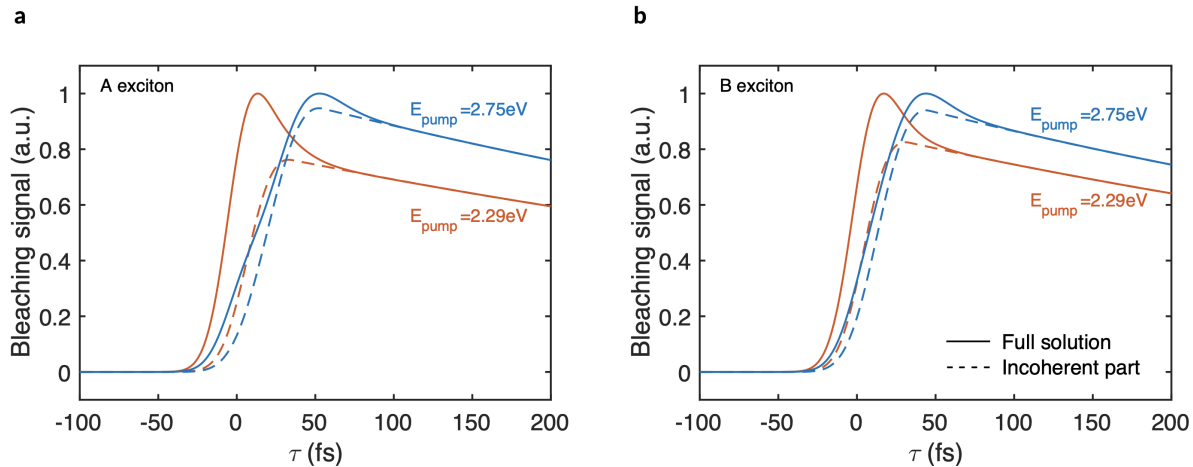


FIG. 4: **Effect of coherent exciton polarization.** a) Calculated $\Delta R/R$ dynamics at the energy of the A_{1s} resonance considering incoherent and coherent contributions (continuous lines) and only the incoherent exciton contribution (dashed lines) for low (orange traces) and high pump photon energy (blue traces). b) The same for the calculated dynamics at the energy of the B_{1s} resonance.

The simulations also capture the occurrence of a sub-100 fs decay component, which is particularly evident in the $\Delta R/R$ temporal trace for the A_{1s} state and progressively vanishes at higher pump photon energies. We attribute this effect to an interplay between a coherent exciton polarization and an incoherent exciton density. The coherent contribution

adiabatically follows the pump pulse and gives rise to an instantaneous coherent build-up, while the incoherent signal is characterized by a delayed formation time. Figure 4 compares the full transient signal incorporating both contributions (solid line) and the signal obtained by artificially turning off the coherent contribution (dashed line) for low and high pump photon energies. For low pump photon energies, the two curves display different dynamics in the first tens of femtoseconds and almost overlap after ~ 100 fs. While the build-up dynamics are dominated by the coherent excitons, the energetically lowest incoherent exciton densities describe the signal after the polarization to population transfer is complete.

For high pump photon energies, the difference between full and incoherent curves diminishes since the coherent part inversely depends on the detuning. This difference is related to the polarization which rapidly decays before a significant 1s exciton density builds up that can be detected by the probe pulse. Thus, the transient signal in this energy regime is strongly dominated by the dynamics of incoherent exciton densities. In this excitation regime, the extracted rise time (~ 30 fs) of the $\Delta R/R$ traces is a direct estimation of the timescale of the incoherent exciton formation process.

Our combined experimental and theoretical work defines a new timescale for the exciton formation process in 1L-TMDs which is much faster than the one previously estimated by intra-excitonic mid-IR [30, 31] and interband visible optical spectroscopy [26]. We also stress that this exciton formation process is faster than the ~ 1 ps trion formation time in TMDs [5] and, remarkably, orders of magnitude faster than the formation time of excitons in quantum wells (i.e. ~ 1 ns) measured by time-resolved photoluminescence [32] and transient terahertz spectroscopy [33]. This result points to a correlation between the formation time and the binding energy of the excitons and suggests that the dynamics of the binding process of electron-hole pairs into excitons is determined by the strength of the exciton binding energy. The reduced Coulomb screening makes this process more rapid and effective than for weakly bound excitons in quantum wells or trions. Two different mechanisms have been proposed to describe the exciton formation process in semiconductors: geminate and bimolecular [34]. In the geminate mechanism excitons are directly created upon photoexcitation by simultaneous emission of optical phonons, while in the bimolecular process, excitons are created from thermalized electron-hole pairs. The observed sub-100-fs build-up dynamics suggests that the geminate mechanism mediated by strong exciton-phonon scattering is the dominant process responsible for the formation of excitons. This conclusion is further supported by

the pump fluence dependent measurements (see Supplementary Fig.S6), where no change of τ_{rise} is observed for different densities of photoexcited excitons, contrary to what expected for a bimolecular formation process.

III. CONCLUSIONS

In summary, we have studied the exciton formation process in 1L-MoS₂ by measuring its transient optical response upon excitation with energy tunable sub-30-fs laser pulses. We resolve an extremely fast and pump photon energy-dependent build-up dynamics of the $\Delta R/R$ signal around the A_{1s} and B_{1s} excitonic transitions. Microscopic calculations of Pauli blocking based on the TMD Bloch equations quantitatively reproduce the experimental results and explain the delayed formation of the transient signal as a result of a phonon-induced cascade-like relaxation process of high-energy incoherent excitons down to the excitonic ground state. These results shed light on the poorly explored mechanism of the exciton formation in 2D semiconductors, redefining the timescale of this process and are extremely important in view of optoelectronic applications of these materials.

References

- [1] T. Mueller and E. Malic. Exciton physics and device application of two-dimensional transition metal dichalcogenide semiconductors. *Npj 2D Materials and Applications* **2**, 29 (2018)
- [2] D. Y. Qiu, F. H. da Jornada and S. G. Louie. Optical Spectrum of MoS₂: Many-Body Effects and Diversity of Exciton States. *Phys. Rev. Lett.* **111**, 216805 (2013).
- [3] K. Yao et al. Optically Discriminating Carrier-Induced Quasiparticle Band Gap and Exciton Energy Renormalization in Monolayer MoS₂. *Phys. Rev. Lett.* **119**, 087401 (2017).
- [4] A. Chernikov et al. Exciton Binding Energy and Nonhydrogenic Rydberg Series in Monolayer WS₂. *Phys. Rev. Lett.* **113** 076802 (2014).
- [5] A. Singh et al. Trion formation dynamics in monolayer transition metal dichalcogenides. *Phys. Rev. B.* **93**, 041401(R) (2016).
- [6] A. Steinhoff et al. Biexciton fine structure in monolayer transition metal dichalcogenides. *Nat. Phys.* **14**, 12, 1199 (2018).
- [7] A. Raja et al. Dielectric disorder in two-dimensional materials. *Nat. Nanotech.* **14**, 832837 (2019).
- [8] J. Kim, X. Hong, C. Jin, S.-F. Shi, C.-Y. S. Chang, M.-H. Chiu, L.-J. Li, F. Wang. Ultrafast generation of pseudo-magnetic field for valley excitons in WSe₂ monolayers. *Science.* **346**, 1205-1208 (2014).
- [9] L. Mennel et al. Optical imaging of strain in two-dimensional crystals. *Nat. Commun.* **9**, 516 (2018).
- [10] J. G. Roch et al. Quantum-Confined Stark Effect in a MoS₂ Monolayer van der Waals Heterostructure. *Nano Lett.* **18**, 10701074 (2018).
- [11] A. V. Stier, K. M. McCreary, B. T. Jonker, J. Kono and S. A. Crooker Exciton diamagnetic shifts and valley Zeeman effects in monolayer WS₂ and MoS₂ to 65Tesla. *Nat. Commun.* **7**, 10643 (2016).
- [12] E. A. A. Pogna et al. Photo-Induced Bandgap Renormalization Governs the Ultrafast Response of Single-Layer MoS₂. *ACS Nano.* **10**, 1, 1182-1188 (2016).
- [13] G. Moody, J. Schaibley, and X. Xu. Exciton dynamics in monolayer transition metal dichalco-

- genides. *J. Opt. Soc. Am. B.* **33**, C39-C49 (2016).
- [14] A. Thnhardt, S. Kuckenburg, A. Knorr, P. Thomas and S. W. Koch. Interplay between coherent and incoherent scattering in quantum well secondary emission. *Phys. Rev. B.* **62**, 16802 (2000).
- [15] M. Kira and S.W. Koch. *Semiconductor Quantum Optics*. Cambridge University Press; 1 edition.
- [16] M. Selig, G. Berghuser, M. Richter, R. Bratschitsch, A. Knorr and E. Malic Dark and bright exciton formation, thermalization, and photoluminescence in monolayer transition metal dichalcogenides. *2D Mater.* **5** 035017 (2018).
- [17] C. Robert et al. Exciton radiative lifetime in transition metal dichalcogenide monolayers. *Phys. Rev. B.* **93**, 205423 (2016).
- [18] Katsch, Florian, Malte Selig, and Andreas Knorr. Theory of coherent pump-probe spectroscopy in monolayer transition metal dichalcogenides. *2D Mater.* **7**, 015021 (2020).
- [19] Glazov, M. M., et al. Exciton fine structure and spin decoherence in monolayers of transition metal dichalcogenides. *Phys. Rev. B.* **89**, 201302 (2014).
- [20] R. Schmidt et al. Ultrafast Coulomb-Induced Intervalley Coupling in Atomically Thin WS₂. *Nano Lett.* **16**, 29452950 (2016).
- [21] S. Dal Conte et al. Ultrafast valley relaxation dynamics in monolayer MoS₂ probed by nonequilibrium optical techniques. *Phys. Rev. B.* **92**, 235425 (2015).
- [22] M. Selig et al. Ultrafast dynamics in monolayer transition metal dichalcogenides: Interplay of dark excitons, phonons, and intervalley exchange. *Phys. Rev. Research.* **1**, 022007(R) (2019).
- [23] M. Massicotte et al. Dissociation of two-dimensional excitons in monolayer WSe₂. *Nat. Commun.* **9**, 1633 (2018).
- [24] Sun, D. et al. Observation of rapid exciton-exciton annihilation in monolayer molybdenum disulfide. *Nano Lett.* **14**, 56255629 (2014).
- [25] Brem, S., Selig, M., Berghaeuser, G. and Malic E. Exciton Relaxation Cascade in two-dimensional Transition Metal Dichalcogenides. *Sci. Rep.* **8**, 8238 (2018).
- [26] F. Ceballos, Q. Cui, M. Z. Bellus and H. Zhao Exciton formation in monolayer transition metal dichalcogenides. *Nanoscale.* **8**, 11681-11688 (2016).
- [27] N. Borys et al. Anomalous Above-Gap Photoexcitations and Optical Signatures of Localized Charge Puddles in Monolayer Molybdenum Disulfide. *ACS Nano.* **11**, 2, 2115-2123 (2017).

- [28] Kira, Mackillo, and Stephan W. Koch. Many-body correlations and excitonic effects in semiconductor spectroscopy. *Progress in quantum electronics* **30**, 5, 155-296 (2006).
- [29] Katsch, Florian, et al. Theory of Exciton-Exciton Interactions in Monolayer Transition Metal Dichalcogenides. *Phys. Stat. Solidi (b)*. **255**, 12, 1800185 (2018).
- [30] P. Steinleitner et al. Direct observation of ultrafast exciton formation in a monolayer of WSe₂. *Nano Lett.* **17**, 14551460 (2017).
- [31] S. Cha et al. 1s-intraexcitonic dynamics in monolayer MoS₂ probed by ultrafast mid-infrared spectroscopy. *Nat. Commun.* **7**, 10768 (2016).
- [32] T. Amand, B. Dareys, B. Baylac, X. Marie, J. Barrau, M. Brousseau, D. J. Dunstan, and R. Planel, Exciton formation and hole-spin relaxation in intrinsic quantum wells *Phys. Rev. B.* **50**, 11624 (1994).
- [33] R. A. Kaindl, M. A. Carnahan, D. Hgele, R. Lvenich, D.S. Chemla Ultrafast terahertz probes of transient conducting and insulating phases in an electron-hole gas. *Nature.* **12**, 423, (6941) (2003).
- [34] C. Piermarocchi, F. Tassone, V. Savona, and A. Quattropani and P. Schwendimann. Exciton formation rates in GaAs/Al_xGa_{1-x}As quantum wells. *Phys. Rev. B.* **55**, 1333, (1997).

IV. METHODS

Sample preparation. The large area 1L-MoS₂ sample was grown by chemical vapor deposition on a SiO₂/Si substrate. The SiO₂ layer thickness is 300nm. The growth procedure was carried on in a dual-zone tube furnace filled by Sulfur and MoO₃ precursors. Further details on the growth process are reported in Ref.[3]. Contrast reflectivity and photoluminescence measurements have been carried out to characterize the static optical response of the sample (see Supplementary Fig.S1)

Pump-probe setup. The ultrafast pump-probe experiments were carried out using a regeneratively amplified Ti:Sapphire system (Coherent Libra II), emitting 100-fs pulses centered at 1.55 eV at 2 kHz repetition rate with 4W average power. The laser drives two home-made Non-collinear Optical Parametric Amplifiers (NOPAs) which serve respectively as the pump and the probe. The first NOPA (probe beam) is pumped at 3.1eV by the second harmonic of the laser and is seeded by a white-light continuum (WLC), generated in a 1-mm-thick sapphire plate. The seed is amplified in a 1-mm-thick beta-barium borate (BBO) crystal and compressed to nearly transform limited duration (i.e. 6 fs) by a pair of custom-designed chirped mirrors. The probe spectrum extends from 1.75 to 2.4 eV, covering the A/B excitonic resonances of 1L-MoS₂. The second NOPA, used to produce the pump beam, is also pumped at 3.1 eV and uses a BBO crystal. It can be configured to amplify either the visible or the near-infrared parts of the WLC. In the former case one obtains pulses tunable from 2 to 2.5 eV, compressed to sub-20-fs duration by chirped mirrors. In the latter case one obtains pulses tunable between 1.25 and 1.4 eV, which are compressed to a nearly transform-limited sub-15-fs duration by a pair of fused silica prisms. These pulses are then frequency-doubled in a 50 μ m-thick BBO crystal to obtain pulses tunable between 2.5 and 2.75 eV. The overall temporal resolution of the setup is characterized via Cross-Frequency Resolved Optical Gating (X-FROG), as extensively explained in Supplementary Note 4. Pump and probe pulses are temporally synchronized by a motorized translation stage, and non-collinearly focused on the sample by a spherical mirror, resulting in spot-size diameters of $\sim 100\mu$ m and $\sim 70\mu$ m, respectively. After the interaction with the pump-excited sample, the probe pulse is spectrally dispersed on a Silicon CCD camera with 532 pixels working at the same repetition rate as the laser. The

pump beam is modulated at 1 kHz by a mechanical chopper. The detection sensitivity is on the order of 10^4 - 10^5 , with an integration time of 2s. The fluence is $\sim 50 \mu\text{J}/\text{cm}^2$ for different pump photon energies (i.e. well below the fluence threshold for the Mott transition measured for 1L-TMDs[1]). No pump fluence dependence of the build-up and the relaxation dynamics was observed upon decreasing the fluence down to $\sim 1 \mu\text{J}/\text{cm}^2$ (see Supplementary Figure 7). In all the experiments, pump and probe beams have parallel linear polarizations. No pump-probe polarization dependence of the build-up dynamics was detected (see Supplementary Figure 6).

Theory. To get insight into the static optical properties of 1L-MoS₂ on SiO₂ substrate, we first solve the Wannier equation, obtaining a set bound and unbound exciton wavefunctions $\varphi_{\nu,q}^{\xi,s}$ with energies $\epsilon_{\nu}^{\xi,s}$. Coherent exciton polarization $P_{\nu}^{\xi,s}$ and incoherent exciton population $N_{\nu_1,\nu_2,P}^{\xi,s}$ are expanded in term of the $\varphi_{\nu,q}^{\xi,s}$ basis, as extensively described in Supplementary Note 7. The dynamic optical response is determined by the TMD Bloch equations for the exciton amplitude including bound and continuum excitonic states [2, 29].

$$\begin{aligned}
& (\partial_t + \gamma_{\nu_1} - \frac{i\epsilon_{\nu_1}^{\xi,s}}{\hbar})P_{\nu_1}^{\xi,s} = \\
& = -i\Omega_{\nu_1}^{\xi,s} + i\sum_{\nu_2,\nu_3,P}\hat{\Omega}_{\nu_2,\nu_3,\nu_1,P}^{\xi,s}[\delta_{P,0}P_{\nu_2}^{\xi,s}(P_{\nu_3}^{\xi,s})^* + \\
& + N_{\nu_2,\nu_3,P}^{\xi,s}] + \frac{i}{\hbar}\sum_{\nu_2,\nu_3,\nu_4}P_{\nu_2}^{\xi,s}P_{\nu_3}^{\xi,s}(P_{\nu_4}^{\xi,s})^* + \\
& + \frac{i}{\hbar}\sum_{\nu_2,\nu_3,\nu_4,P}\hat{V}_{\nu_2,\nu_3,\nu_4,\nu_1,P}^{\xi,s}P_{\nu_2}^{\xi,s}N_{\nu_3,\nu_4,P}^{\xi,s}.
\end{aligned} \tag{1}$$

The left-hand side of Eq.1 describes the oscillation of the exciton transition damped by a dephasing rate γ_{ν_1} [3, 4]. The first term on the right-hand side represents the optical pump generating excitons with zero center-of-mass motion at the corners of the hexagonal Brillouin zone with σ_+ ($\xi=K$) or σ_- ($\xi=K'$) circularly polarized light. The excitonic Rabi frequency is defined as: $\Omega_{\nu_1}^{\xi,s} = \frac{1}{\hbar}\sum_q d_{\epsilon,s,q}^{\nu,c} \cdot E(t)\varphi_{\nu_1,q}^{\xi,s}$, where $d_{\epsilon,s,q}^{\nu,c}$ is the dipole matrix element and $E(t)$ the exciting light field. The next contribution characterizes Pauli blocking by coherent excitons ($|P|^2$) and incoherent densities (N) resulting in a suppression of the excitonically modified

Rabi frequency:

$$\hat{\Omega}_{\nu_2, \nu_3, \nu_1, P}^{\xi, s} = \sum_q d_{\epsilon, s, q}^{\nu, c} \cdot \frac{E(t)}{\hbar} \cdot (\varphi_{\nu_2, q + \beta_{\xi, s} P}^{* \xi, s} \varphi_{\nu_3, q + \beta_{\xi, s} P}^{\xi, s} + \varphi_{\nu_2, q - \alpha_{\xi, s} P}^{* \xi, s} \varphi_{\nu_3, q - \alpha_{\xi, s} P}^{\xi, s}) \varphi_{\nu_1, q}^{\xi, s}. \quad (2)$$

The last two terms on the right-hand side of Eq.1 characterize Coulomb interactions through exciton-exciton scattering:

$$V_{\nu_2, \nu_3, \nu_1, P}^{\xi, s} = \sum_{q_1, q_2} \frac{V_{q_1 - q_2}}{\epsilon_{q_1 - q_2}} \varphi_{\nu_2, q_1}^{* \xi, s} \varphi_{\nu_3, q_2}^{* \xi, s} \cdot (\varphi_{\nu_4, q_1}^{\xi, s} - \varphi_{\nu_4, q_2}^{\xi, s}) (\varphi_{\nu_1, q_1}^{\xi, s} - \varphi_{\nu_1, q_2}^{\xi, s}). \quad (3)$$

In order to decrease the complexity of the problem for the description of the experiment, the excitonic occupations N are treated with effective occupation numbers ν , averaging over the details of the complex momentum dispersion of incoherent exciton densities: $\sum_{\nu_2, \nu_3, P} \hat{\Omega}_{\nu_2, \nu_3, \nu_1, P}^{\xi, s} N_{\nu_2, \nu_3, P}^{\xi, s} \approx \sum_{\nu_2} \tilde{\Omega}_{\nu_2, \nu_1}^{\xi, s} N_{\nu_2}^{\xi, s}$ with $\tilde{\Omega}_{\nu_2, \nu_1}^{\xi, s} / \hat{\Omega}_{\nu_2, \nu_2, \nu_1, 0}^{\xi, s} = 0.55$ for $\{\xi, s\} = \{K, \uparrow\}$, $\{K', \downarrow\}$ and 0.25 for $\{\xi, s\} = \{K, \downarrow\}$, $\{K', \uparrow\}$.

However, the bleaching cross sections are explicitly evaluated as a function of the exciton state number ν . These cross sections exhibit a drastic decrease with increasing state number. The equations of motion of the exciton densities are given by:

$$(\partial_t + \Gamma_{decay}) N_{1s}^{\xi, s} = 2\gamma_{1s}^{\xi, s} |P_{1s}^{\xi, s}|^2 + \Gamma_{2s \rightarrow 1s}^{\xi, s} N_{2s}^{\xi, s}, \quad (4)$$

$$(\partial_t + \Gamma_{\nu \rightarrow \nu-1}^{\xi, s}) N_{\nu}^{\xi, s} = 2\gamma_{\nu}^{\xi, s} |P_{\nu}^{\xi, s}|^2 + \Gamma_{\nu+1 \rightarrow \nu}^{\xi, s} N_{\nu+1}^{\xi, s}. \quad (5)$$

Eqs.(4) and (5) describe the dynamics of the incoherent exciton densities associated with the energetically lowest 1s state $N_{1s}^{\xi, s}$ and higher states $N_{\nu}^{\xi, s}$, respectively. $\Gamma_{decay} = 1 \text{meV}/\hbar$ characterizes the relaxation of the incoherent exciton densities into the ground state; its value is adjusted to the experimental results. The first contribution on the right-hand side of Eqs (4) and (5) represent the formation of incoherent exciton densities out of optically excited coherent excitations by exciton-phonon scattering [5, 25], whereas the terms proportional to $\Gamma_{\nu+1 \rightarrow \nu}^{\xi, s}$ characterize the phonon-mediated relaxation from energetically higher densities with effective rates $\Gamma_{\nu+1 \rightarrow \nu}^{\xi, s} = \frac{1eV}{50fs} \frac{1}{\epsilon_{\nu+1}^{\xi, s} - \epsilon_{\nu}^{\xi, s}}$ adapted to density functional theory calculations [6, 7]. Solving the set of equations of motion, Eqs.(1), (4) and (5) for the blocking contribution gives access to the measured differential absorption signal calculated as: $\Delta\alpha(\tau) = \alpha_{p,t}(\tau) - \alpha_t$, where $\alpha_{p,t}(\alpha_t)$ are the absorption coefficients of the pumped (unpumped) 1L-MoS₂. The numerical results are obtained only by taking into account the Pauli blocking effect. However, the incoherent Coulomb renormalizations in the TMD Bloch equations, originating

from incoherent exciton populations, are formed on a similar time scale. Exciton binding energy renormalization and other many-body effects related to the transient variation of the Coulomb screening are not considered in the model. The agreement between the calculated and measured dynamics strongly suggests that the out-of-equilibrium optical response of 1L-MoS₂ on a sub-100 fs timescale is well captured by considering only population effects such as phase-space filling.

Acknowledgments

We thank Dominik Christiansen for many stimulating discussions. We gratefully acknowledge funding from the Deutsche Forschungsgemeinschaft via the projects KN 427/11-1 (F.K. and A.K.) as well as 182087777 -SFB 951 (B12, M.S., A.K.). We also acknowledge support of the European Union's Horizon 2020 research and innovation program under Grant Agreement No. 734690 (SONAR, A.K. and F.S.). This project has received funding from the European Unions Horizon 2020 research and innovation program under the Marie Skłodowska-Curie (grant agreement no. 734690) and from the European Research Council (ERC, grant agreement no. 816313- F.S.). G.C. and S.D.C acknowledges support by the European Union Horizon 2020 Programme under Grant Agreement No. 785219 Graphene Core 2. S.D.C. and C.T acknowledge financial support from MIUR through the PRIN 2017 Programme (Prot. 20172H2SC4). P.J.S. and K.Y. acknowledge support from Programmable Quantum Materials, an Energy Frontier Research Center funded by the U.S. Department of Energy (DOE), Office of Science, Basic Energy Sciences (BES), under award de-sc0019443. Work at the Molecular Foundry was supported by the Office of Science, Office of Basic Energy Sciences, of the U.S. Department of Energy under Contract No. DE-AC02-05CH11231. This research was supported in part by the U.S. Department of Energy, Office of Science, Office of Basic Energy Sciences, Materials Sciences and Engineering Division under Contract No. DE-AC02-05-CH11231, within the van der Waals Heterostructures Program (KCWF16), which provided for sample growth, and under the sp²-bonded Materials Program (KC2207), which provided for SEM sample characterization (A.Z. and A.Y.). Support was also provided by the U.S. National Science Foundation under Grant No. DMR-1807233 which provided for additional TEM sample characterization (A.Z. and A.Y.).

References

- [1] A. Chernikov, C. Ruppert, H. M. Hill, A. F. Rigosi and T. F. Heinz. Population inversion and giant bandgap renormalization in atomically thin WS₂ layers. *Nat. Photonics* **9**, 466470 (2015).
- [2] Lindberg, M., and Stephan W. Koch. Effective Bloch equations for semiconductors. *Phys. Rev. B.* **38**, 5, 3342 (1988).
- [3] Selig, Malte, et al. Excitonic linewidth and coherence lifetime in monolayer transition metal dichalcogenides. *Nat. Comm.* **7**, 13279 (2016).
- [4] Christiansen, Dominik, et al. Phonon sidebands in monolayer transition metal dichalcogenides. *Phys. Rev. Lett.* **119**, 18, 187402 (2017).
- [5] Selig, Malte, et al. Quenching of Intervalley Exchange Coupling in the Presence of Momentum-Dark States in TMDCs. arXiv preprint *arXiv:1908.11178*. (2019).
- [6] Li, Xiaodong, et al. Intrinsic electrical transport properties of monolayer silicene and MoS₂ from first principles. *Phys. Rev. B.* **87**, 11, 115418 (2013).
- [7] Jin, Zhenghe, et al. Intrinsic transport properties of electrons and holes in monolayer transition-metal dichalcogenides. *Phys. Rev. B.* **90**, 4, 045422 (2014).